Check for updates

Laser & Photonics Reviews

LASER & PHOTONICS REVIEWS

www.lpr-journal.org

RESEARCH ARTICLE

Lines of Bound States in the Continuum in Monodisperse Microsphere Structures

Benjamin Cerjan[1] | Alexander Cerjan[2]

[1]Department of Chemistry, Purdue University, West Lafayette, Indiana, USA | [2]Center for Integrated Nanotechnologies, Sandia National Laboratories, Albuquerque, New Mexico, USA

Correspondence: Alexander Cerjan (awcerja@sandia.gov)

Received: 17 August 2025 | **Revised:** 23 October 2025 | **Accepted:** 17 November 2025

Keywords: bound states in the continuum | microspheres | photonic crystals

ABSTRACT

Incorporating epitaxially grown active semiconductor media into self-assembled microsphere crystals has remained a major challenge as the curved geometry of the spheres is incompatible with conventional planar growth and patterning techniques. As a result, active photonic devices based on such self-assembled structures, which have other desirable properties such as enabling the rapid assembly of large area systems, have been elusive. Here, we numerically demonstrate an alternative route to creating high-Q resonances in microsphere-based nanophotonic assemblies compatible with standard optical gain materials. We show that close-packed layers of monodisperse microspheres can exhibit symmetry bandgaps, regardless of their layer stacking order. Thus, this microsphere environment can be used to create lines of bound states in the continuum (BICs) of an embedded slab made of active material. Using a realistic ZnS@SiO_2 (core-shell) architecture and sphere diameters compatible with scalable colloidal assembly, we predict sharp spectral features in angle-resolved transmission that trace these lines of BICs and persist in the presence of some fabrication disorder. Altogether, in enabling the integration of unpatterned epitaxial gain slabs with large-area colloidal microsphere assemblies, this approach opens a practical path toward active, dynamically reconfigurable photonic devices that leverage BIC physics for narrow-linewidth lasing and enhanced light–matter interactions.

1 | Introduction

The self-assembly of monodisperse microspheres into ordered optical structures has garnered significant interest due to its potential for scalable, cost-effective fabrication of functional materials. Unlike traditional nanofabrication methods for photonic devices operating at optical and telecommunications wavelengths, which can require complex growth and etching processes, microsphere-based materials can be chemically assembled through a variety of techniques, including dip-coating [1–3], spin-coating [4–6], electrophoretic deposition [7–9], Langmuir–Blodgett deposition [10, 11], and colloidal epitaxy–methods [12] that allow for large-scale formation of ordered structures with tunable properties [13, 14]. When organized into three-dimensional crystals or their inverse structures, such colloidal-based systems can exhibit complete photonic bandgaps [15–18], prohibiting the propagation of light in any direction for a range of wavelengths determined by the microsphere radius and index of refraction. Likewise, disordered or amorphous structures can exhibit structural color [19–24], resulting in wavelength- and angle-dependent reflectivity.

Beyond realizing control over linear electromagnetic phenomena, significant progress has also been made in enhancing light-matter interactions within three-dimensional colloidal photonic crystals. By incorporating active emitters such as dye molecules [25–27] or quantum dots [28–30] into the colloidal matrix, both spontaneous emission and lasing have been demonstrated. These

© 2025 Wiley-VCH GmbH

developments underscore the potential of colloidal self-assembly as a route to scalable and cost-effective active photonic materials. However, despite these advances, achieving seamless integration of colloidal photonic crystals with traditional III-V semiconductor gain media that forms the backbone of high-performance optoelectronic devices remains an outstanding challenge. The key difficulty lies in the fact that microspheres made from active semiconductor materials typically suffer from edge recombination losses, while the epitaxial growth techniques for achieving optical gain are incompatible with infiltration into pre-formed colloidal structures. As a result, new strategies are required to bridge this materials gap and unlock the full potential of combining colloidal photonic crystals with semiconductor gain media.

Here, we propose and numerically demonstrate an alternative route to creating high-quality (Q) resonances for enhancing light-matter interactions using colloidal photonic crystals that is compatible with epitaxially grown III-V semiconductor gain media. Specifically, we show that a solid slab embedded within an environment formed by a colloidal assembly of close-packed monodisperse microspheres can support lines of bound states in the continuum (BICs) [31–35] due to the three-fold rotational symmetry of the colloidal environment with respect to the embedded slab. For perfectly close-packed structures, these lines of BICs remain robust regardless of whether the microspheres are arranged in hexagonal close-packed (HCP), face-centered cubic (FCC), or randomly stacked layers, as all layer configurations maintain the same threefold symmetry, ensuring that our results are compatible with standard colloidal assembly processes. Furthermore, because the gain slab remains unpatterned and can be positioned atop a Bragg stack for single-sided operation, our design is compatible with conventional semiconductor fabrication methods and motifs. Looking forward, our results point to the construction of dynamically reconfigurable, large-area, high-Q photonic devices using colloidal-based systems for enhancing light-matter interactions.

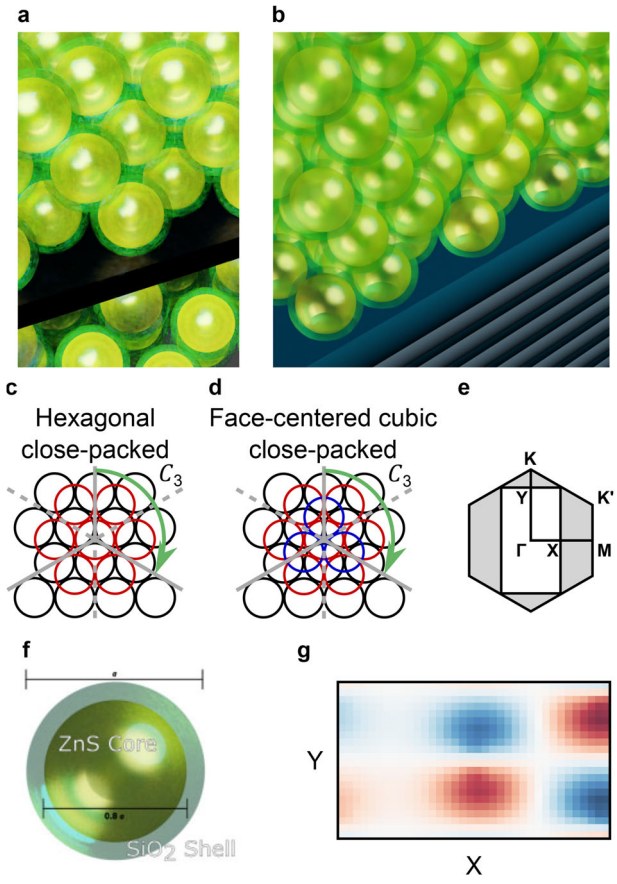


FIGURE 1 | a) FCC lattice of spheres with an embedded slab that breaks the system's translational symmetry in the vertical direction. b) FCC lattice of spheres on a slab on top of a Bragg reflector. c,d) Schematics of the constituent layers of an HCP lattice (c) and FCC lattice (d) showing that both structures have preserved in-plane reflection and rotation symmetries even when the vertical translational symmetry is broken. e) Schematic of the 2D reduced Brillouin zone considered, as well as the computational supercell's Brillouin zone, with high-symmetry points marked. f) Shows a single sphere with a ZnS core of radius $0.4a$ and SiO_2 shell of radius $0.5a$ where a is the distance between the centers of two spheres. g) E_z field profile inside the slab at $z = 0.1a$ sliced in the x-y plane for incident light $\omega = 0.5775\ (2\pi c/a)$ and $\mathbf{k}_{\parallel} = (0.8, 0, 0)\pi/a$.

2 | Theory of Lines of BICs Originating From Symmetry Bandgaps

Traditionally, BICs in nanophotonic systems have been studied in planar structures that are open to free space (or some other homogeneous medium) on at least one side, such as photonic crystal slabs and metasurfaces [36]. In such systems, BICs can form through a few different mechanisms, e.g., via symmetry protection [37–42], a Friedrich–Wintgen process [43, 44], and accidentally [45, 46]. However, regardless of the specific formation mechanism, any BICs in planar structures open to free space appear as isolated points with infinite Q in frequency-wavevector space $(\omega, \mathbf{k}_{\parallel})$ [34], whose locations are controlled by the geometry of the planar structure. As such, there are limited degrees of freedom available to control such systems via any introduced passive colloidal particles.

Instead, to create BICs in structures formed using close-packed monodisperse microspheres, we turn to a light-trapping mechanism based on tailoring the radiative environment surrounding a subsystem [34]. Consider a slab embedded in an environment of close-packed spheres, with the spheres either on both sides of the slab, as shown in Figure 1a, or only on a single side of the slab that is atop a dielectric mirror, Figure 1b. When layers of close-packed spheres are stacked on top of each other, the layers can come in three different orientations, see Figure 1c,d. Alternating between two such layer types creates a hexagonal close-packed (HCP) lattice, see Figure 1c, while a cyclic ordering of all three layer types creates a face-centered cubic (FCC) close-packed lattice, see Figure 1d. From the perspective of the embedded slab, both HCP and FCC stackings have preserved C_{3v} symmetry, where the C_3 (i.e., 120°) rotations are taken about an axis perpendicular to the slab and the reflection symmetries R are about planes that are similarly perpendicular to the slab. Note that the existence of the slab breaks any such spatial symmetries in the out-of-plane direction. Crucially, even an arbitrary arrangement of close-packed layer configurations preserves this same in-plane C_{3v} point group symmetry, as the HCP and FCC lattices share the same out-of-plane axes and planes that underpin their C_{3v} symmetry.

The existence of the in-plane C_{3v} point group symmetry, regardless of stacking arrangement, means that close-packed monodisperse microspheres can exhibit symmetry bandgaps [34] along high-symmetry lines that preserve a reflection symmetry. To elaborate on how a symmetry bandgap can manifest, consider the source-free Maxwell's wave equation for in-plane periodic dielectric media $\varepsilon(\mathbf{x})$,

$$\Theta(\mathbf{k}_\parallel)\mathbf{u}_{n,\mathbf{k}_\parallel}(\mathbf{x}) = \frac{\omega^2_{n,\mathbf{k}_\parallel}}{c^2}\varepsilon(\mathbf{x})\mathbf{u}_{n,\mathbf{k}_\parallel}(\mathbf{x}), \tag{1}$$

where

$$\Theta(\mathbf{k}_\parallel) = (\nabla + i\mathbf{k}_\parallel)\times\mu^{-1}(\nabla + i\mathbf{k}_\parallel)\times. \tag{2}$$

Here, $\mathbf{u}_{n,\mathbf{k}_\parallel}(\mathbf{x})$ is the nth Bloch wavefunction at in-plane wavevector $\mathbf{k}_\parallel = (k_x, k_y, 0)$ for the electric field $\mathbf{E}_{n,\mathbf{k}_\parallel}(\mathbf{x}) = e^{i\mathbf{k}_\parallel\cdot\mathbf{x}}\mathbf{u}_{n,\mathbf{k}_\parallel}(\mathbf{x})$ with frequency $\omega_{n,\mathbf{k}_\parallel}$, and μ is the magnetic permeability that is assumed to be spatially uniform. Moreover, let the dielectric distribution possess a reflection symmetry about the $y = 0$ plane, such that $R_y : (x, y, z) \mapsto (x, -y, z)$ and $\varepsilon(R_y^{-1}\mathbf{x}) = \varepsilon(\mathbf{x})$. Even though the underlying dielectric structure possesses this spatial symmetry, $\Theta(\mathbf{k}_\parallel)$ only exhibits this symmetry along high-symmetry lines in wavevector space such as **Γ–X** where $k_y = 0$, such that $[\Theta(k_x\hat{\mathbf{x}}), R_y] = 0$, see Figure 1e, where $\hat{\mathbf{x}} = (1, 0, 0)$. Thus, along **Γ–X**, all of the system's eigenstates can be constructed to be simultaneous eigenstates of R_y, such that every $\mathbf{u}_{n,k_x\hat{\mathbf{x}}}(\mathbf{x})$ is either even or odd under this symmetry,

$$R_y\mathbf{u}_{n,k_x\hat{\mathbf{x}}}(\mathbf{x}) = \pm\mathbf{u}_{n,k_x\hat{\mathbf{x}}}(\mathbf{x}), \tag{3}$$

as $R_y^2 = I$ such that its eigenvalues are limited to ±1, and where I is the identity. For an infinite stacking of arbitrary layers of monodisperse close-packed microspheres, it may happen that, along a high-symmetry line such as **Γ–X**, a range of frequencies appears in which every eigenstate $\mathbf{u}^{(\text{sphere})}_{n,k_x\hat{\mathbf{x}}}(\mathbf{x})$ possesses the same reflection eigenvalue; for example, every eigenstate in this frequency range is even, $R_y\mathbf{u}^{(\text{sphere})}_{n,k_x\hat{\mathbf{x}}}(\mathbf{x}) = \mathbf{u}^{(\text{sphere})}_{n,k_x\hat{\mathbf{x}}}(\mathbf{x})$. Thus, this close-packed sphere photonic crystal possesses a symmetry bandgap.

Having identified a mechanism by which photonic crystals created from close-packed sphere structures can form symmetry bandgaps, it is straightforward to create a line of BICs within the solid slab embedded inside the microsphere radiative environment. If a uniform slab is embedded into such a photonic crystal along the $z = 0$ plane (Figure 1a), there may be modes that are predominantly confined to the slab $\mathbf{u}^{(\text{slab})}_{n,\mathbf{k}_\parallel}(\mathbf{x})$. As the combined structure retains the reflection symmetry R_y, any such slab-localized resonances must also obey Equation (3) along **Γ–X**. By tuning the height of the slab, one can overlap a slab resonance band with a symmetry bandgap, such that the slab resonance and the available microsphere environment channels at the same frequency transform in opposite ways under R_y. If the microsphere radiative environment extends to infinity, such a band of slab resonances becomes completely trapped along the high-symmetry line as the coupling rate between a slab-localized state and a surrounding microsphere environment channel [47, 48] necessarily vanishes

$$\gamma_{mn} \propto \int \left(\mathbf{u}^{(\text{sphere})}_{m,k_x\hat{\mathbf{x}}}(\mathbf{x})\right)^* \cdot \mathbf{u}^{(\text{slab})}_{n,k_x\hat{\mathbf{x}}}(\mathbf{x})d^3\mathbf{x}. \tag{4}$$

Altogether, such a slab resonance tuned to reside in a symmetry bandgap results in a line of BICs along the high-symmetry line.

Symmetry bandgaps are distinguished from their conventional bandgap counterparts because they allow for the propagation of waves that are symmetry-matched, as opposed to disallowing all propagation within the bandgap. However, there is another key difference in how these features can change as $\mathbf{k}_\parallel$ is varied off of the high-symmetry line. Consider a symmetry bandgap and a regular-but-incomplete bandgap of equal widths along a high-symmetry line. As $\mathbf{k}_\parallel$ is varied off of the high-symmetry line, the symmetry bandgap closes immediately, as the conditions for its formation have been simultaneously broken for the entire frequency range. Moreover, off the high-symmetry line, the decay rate of any trapped resonance can be found using a $\mathbf{k}\cdot\mathbf{p}$ approximation by expanding $\Theta(\mathbf{k}_\parallel)$ in the vicinity of the high-symmetry line. If the high-symmetry line is along **Γ–X** such that $(0, \delta k_y, 0)$ is a small perturbation away from the line,

$$\Theta(k_x\hat{\mathbf{x}} + \delta k_y\hat{\mathbf{y}}) \approx \Theta(k_x\hat{\mathbf{x}}) + \delta k_y \left.\frac{\partial\Theta}{\partial k_y}\right|_{k_x\hat{\mathbf{x}}} + \mathcal{O}(\delta k_y^2), \tag{5}$$

in which the effective perturbation is

$$\left.\frac{\partial\Theta}{\partial k_y}\right|_{k_x\hat{\mathbf{x}}} = i\hat{\mathbf{y}}\times\mu^{-1}(\nabla + ik_x\hat{\mathbf{x}})\times + (\nabla + ik_x\hat{\mathbf{x}})\times i\mu^{-1}\hat{\mathbf{y}}\times, \tag{6}$$

where $\hat{\mathbf{y}} = (0, 1, 0)$ and we are ignoring terms depending on δk_y^2 or higher powers.

Using this expansion of Maxwell's equations, we can project into a two-component subspace comprised of a slab resonance and microsphere environment channel that have the same frequency $\omega_0(k_x\hat{\mathbf{x}})$ and $\mathbf{k}_\parallel$, formed from $[\mathbf{u}^{(\text{slab})}_{n,k_x\hat{\mathbf{x}}}(\mathbf{x}), \mathbf{u}^{(\text{sphere})}_{m,k_x\hat{\mathbf{x}}}(\mathbf{x})]^\top$, yielding the effective Hamiltonian

$$H_{\text{eff}}(k_x, \delta k_y) = \begin{bmatrix} \omega_0(k_x\hat{\mathbf{x}}) & \delta k_y g \\ \delta k_y g^* & \omega_0(k_x\hat{\mathbf{x}}) \end{bmatrix}, \tag{7}$$

in which

$$g = \frac{c^2}{2\omega_0}\int \left(\mathbf{u}^{(\text{sphere})}_{m,k_x\hat{\mathbf{x}}}(\mathbf{x})\right)^* \cdot \left.\frac{\partial\Theta}{\partial k_y}\right|_{k_x\hat{\mathbf{x}}} \mathbf{u}^{(\text{slab})}_{n,k_x\hat{\mathbf{x}}}(\mathbf{x})d^3\mathbf{x}. \tag{8}$$

Note that $\partial\Theta/\partial k_y|_{k_x\hat{\mathbf{x}}}$ is odd under R_y, as the dependence on d/dy disappears in the cross product, while $\hat{\mathbf{y}} \mapsto -\hat{\mathbf{y}}$. Therefore, this perturbation does not affect the diagonal elements of H_{eff}, as it can only yield a nonzero contribution between two states with opposite behavior under R_y. Finally, we can use Fermi's golden rule to find the radiative decay rate of the slab resonance

$$\gamma_{\text{rad}} = 2\pi\delta k_y^2|g|^2\rho(\omega_0), \tag{9}$$

showing that, to leading order, any slab resonance that is a BIC along the high-symmetry line due to the symmetry bandgap acquires a decay rate proportional to δk_y^2 away from the high-symmetry line. Here, $\rho(\omega_0)$ is the density of states at ω_0. In contrast, an ordinary incomplete bandgap of equal width where there is no microsphere environmental channel at the same frequency and $\mathbf{k}_\parallel$ at the slab resonance can only close so quickly,

guaranteeing a range of δk_y where no environmental channel exists and the radiative decay rate vanishes. Thus, relative to conventional bandgaps, symmetry bandgaps produce substantially sharper spectral features.

3 | Lines of BICs in Monodisperse Microspheres

Here, we consider a readily-fabricatable system capable of supporting lines of BICs composed of ZnS@SiO_2 (core-shell) microspheres assembled on a TiO_2 substrate [49], designed to operate near $\lambda = 633$ nm. As diagrammed in Figure 1f, our microsphere 3D photonic crystal is composed of nanoparticles with a core diameter of $0.8a$ and a shell thickness of $0.1a$, where a is the size of a unit cell (i.e., such that the full microsphere diameter is a). Embedded within this environment is a TiO_2 slab with thickness $0.34a$, chosen so that a transverse magnetic-like (TM-like) family of slab-localized resonances exists near $\lambda = 633$ nm. An example of such a slab-localized resonance embedded in a FCC environment with $\mathbf{k}_{\|}$ along the **Γ–X** high-symmetry line is shown in Figure 1g, demonstrating odd symmetry about $y = 0$ and thus confirming that this family of slab resonances along the high-symmetry line are also eigenstates of R_y. For the design wavelength of 633 nm, this corresponds to a total microsphere diameter of $a = 367$ nm, such that the core diameter is ~ 294 nm, shell thickness of ~ 37 nm, and a slab thickness of ~ 125 nm.

An analysis of the ZnS@SiO_2 3D photonic crystal modes supported by both FCC and HCP arrangements of the microspheres, and in the absence of the TiO_2 slab "subsystem," reveals that along the **Γ–X** high-symmetry line both crystalline structures exhibit a symmetry bandgap. These results form the background in Figure 2a,b where red indicates frequencies where odd modes are supported and green indicates even modes are supported by the environment for any k_z. In particular, both environment structures possess a region in (ω, k_x)-space where only even modes exist. Moreover, the symmetry bandgap persists even upon mixing the two different arrangements of close-packed spheres, see Figure 2c.

Within the symmetry bandgap, the subsystem introduced by the TiO_2 slab can support BICs that do not radiate as they correspond to an in-plane symmetry that does not exist in the surrounding environment, see Figure 2d,e. By truncating the microsphere environment to be a few layers thick, the line of BICs becomes a line of quasi-BICs that can be either probed from the free-space far-field, or radiate to the free-space far-field if the slab contains a gain medium. To find the line(s) of high-Q slab resonances in such a truncated environment, simulations were performed with a dipole source inside the slab defect and harmonic inversion was used to find the resulting frequencies and Q-factors as a function of k_x, see Figure 2. Along these high-symmetry lines, the slab resonances exhibited numerical Q-factors $\geq 10^5$, indicating strong confinement to the slab. Additionally, all three environment conditions reveal the dispersion of the high-Q states, showing the potential for tuning the frequency of the response via the adjustment of incident angle of the light.

To demonstrate that these modes form a line of BICs only along the system's high-symmetry lines and become resonances immediately as their wavevector shifts off of the high-symmetry

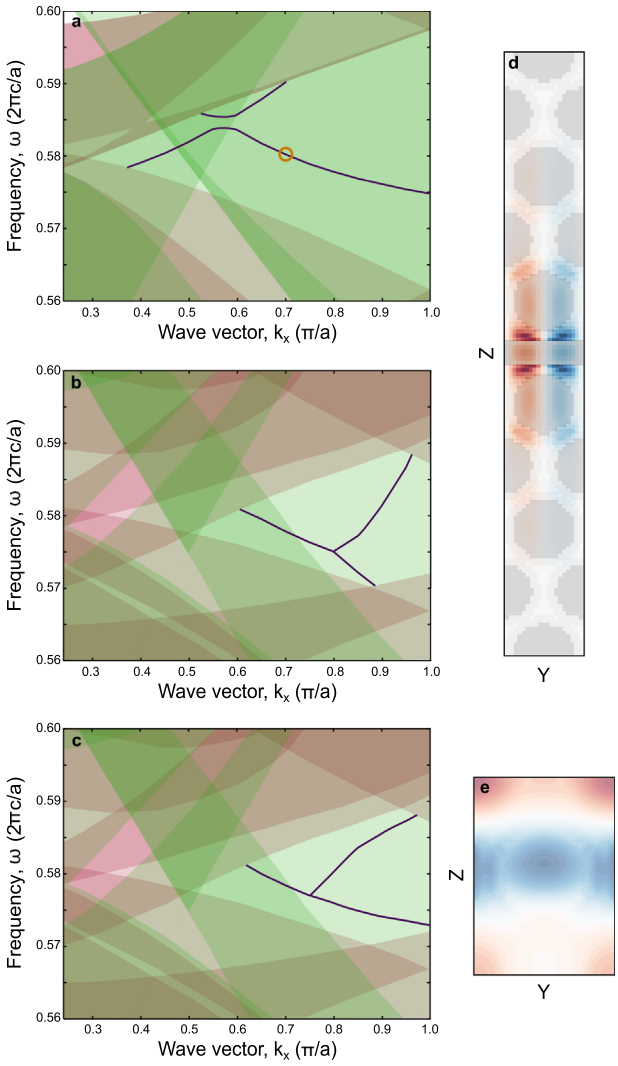


FIGURE 2 | Environment modes and lines of BICs within each for (a) HCP lattice, (b) FCC lattice, and (c) mixed FCC/HCP layers. Green indicates even modes are supported in the environment while red indicates odd modes are supported. The purple lines indicate high-Q ($> 10^5$) modes that exist within the slab but do not radiate into the surrounding truncated environment. (d,e) E_z in the yz-plane for the slab-localized resonance in an HCP environment (d) shown in (b) at $k_x = 0.7\pi/a$, indicated by the orange circle, and the HCP environment channel at the same frequency and k_x (e).

line, we show numerical transmission spectrum results for slight wavevector detunings about the **Γ–X** line away from $k_y = 0$ in Figure 3. Away from $k_y = 0$, a clear Fano resonance spectral signature is seen that slowly narrows and finally disappears at the high-symmetry line, see Figure 3a,b. The disappearance of this Fano feature occurs at nearly exactly the same frequency as predicted using an embedded dipole source, confirming the resonances high-Q along the high-symmetry line. Moreover, this spectral feature appears regardless of the number of microsphere layers (compare Figure 3a,b), both indicating that this feature corresponds to a slab-localized state and also illustrating how the line of BICs can be probed using transmission spectra. Upon removal of the slab from the system (Figure 3c), this entire spectral feature disappears, providing further evidence that the Fano feature's presence in Figure 3a,b is connected to the

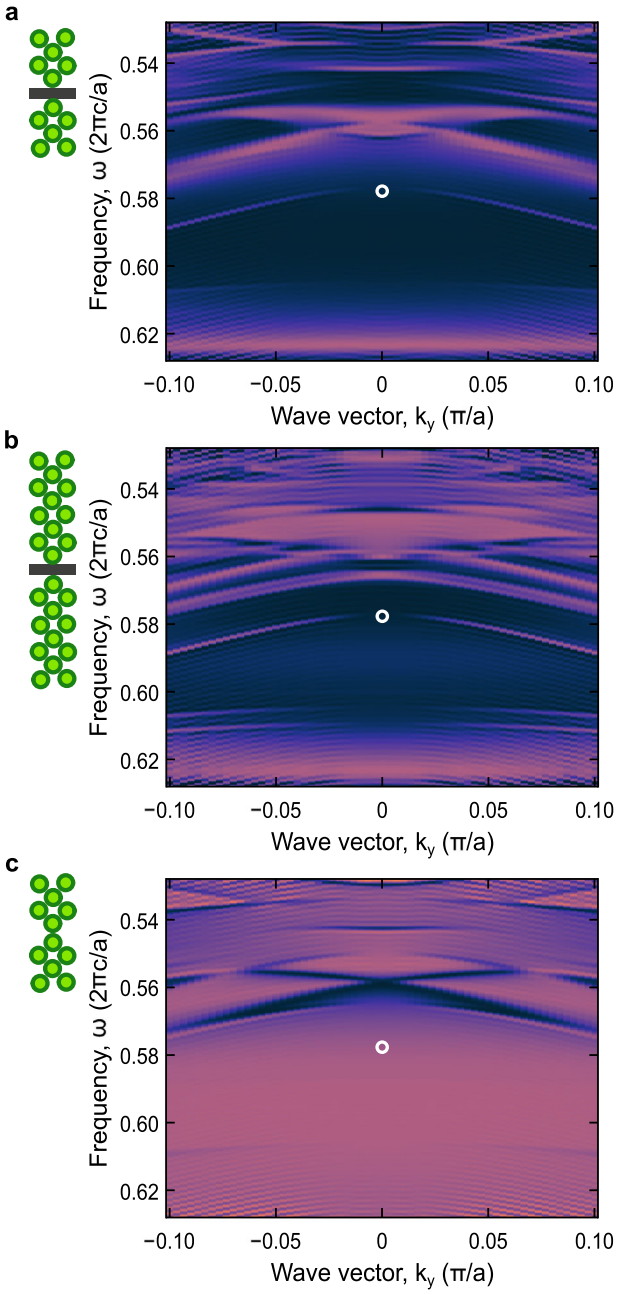


FIGURE 3 | Transmission spectra as a function of tuning across $k_y = 0$, for 6 single-microsphere-thick layers of HCP-stacked spheres on both sides of slab (a), 12 layers (b), and 6 layers without the slab (c). Input light is p-polarized at $k_x = 0.8\pi/a$. All are on the same color scale with arbitrary units. A full unit cell in the vertical direction of HCP microspheres consists of two layers. The white circles are the predicted location of the BIC from the FDTD simulations in Figure 2. Insets show the simulated system schematically.

embedded slab. Note, the modes are only seen for p-polarized input light due to the symmetry requirements of these modes. Overall, these simulations not only confirm the presence of a BIC along the high-symmetry line, but illustrate the sharpness of its spectral signature following Equation (9).

Finally, to establish that there is a full line of BICs using transmission simulations, we calculate the transmission spectra for a fixed number of layers across a range of incident choices of k_y in the vicinity of the high-symmetry line and for a few different choices of k_x, as shown in Figure 4. For every such choice of k_x, we numerically observe the same characteristic Fano feature for $k_y \neq 0$, while the Fano feature vanishes at $k_y = 0$, demonstrating an entire line of BICs with varying modal frequencies throughout the symmetry bandgap of the environment. The disappearance of the spectral feature also shows strong agreement with the frequency of the BIC as predicted using an embedded source.

Overall, the dimensions of the colloidal ZnS@SiO_2 microspheres we consider are well within established methods for synthesizing such particles [49, 50]. Moreover, such microspheres have been used for a variety of optical applications via a range of methods for self-assembly into close-packed layers [49–51]. Thus, making a photonic structure on a Bragg reflector, as shown in Figure 1b would be a straightforward application of previously developed techniques with a Bragg reflector as the substrate. In contrast, making the structure in Figure 1a would be more involved, requiring a backside etch to expose a thin membrane of TiO_2 before assembling spheres on either side of the substrate and likely involving including small additional structural features to force the microspheres on either side of the slab to be mirror-symmetric with respect to the slab.

Heuristically, the core-shell geometry we are using creates a photonic crystal that is attempting to approximate suspended, disconnected high-index spheres that maintain a crystalline structure. Thus, we expect that as microsphere synthesis methods are able to incorporate more materials with a wider range of refractive indexes, the width of the symmetry bandgap and its length in wavevector space can be substantially expanded. Simulations show that by increasing the refractive index of the core material or decreasing the index of the shell material, even without changing the relative radius or thickness of the core-shell microspheres, can significantly broaden the symmetry bandgap of close-packed microsphere structures, see Figure 5. Thus, the ability to fabricate microspheres whose cores were, e.g., GaP, would yield a much larger index contrast in the core-shell microspheres and would greatly increase the operating range of these proposed structures.

4 | Effects of Structural Perturbations

In any realistic implementation, colloidal microsphere assemblies will inevitably depart from perfect periodicity. Even with state-of-the-art fabrication, microsphere diameters will vary slightly, stacking faults will arise, and so the long-range order will only be approximate. Such imperfections break the exact reflection symmetries that underlie the ideal lines of BICs that we consider, raising the concern that the resulting resonances could degrade into ordinary low-Q modes. However, it is important to emphasize that the relevant benchmark is not the near-infinite Q of a perfect structure, but rather the Q factors achieved in current active optical devices. For example, state-of-the-art metasurfaces or patterned semiconductor resonators typically reach Q values only in the few hundreds to low thousands, yet are sufficient to support lasing and nonlinear optical functionalities [52, 53].

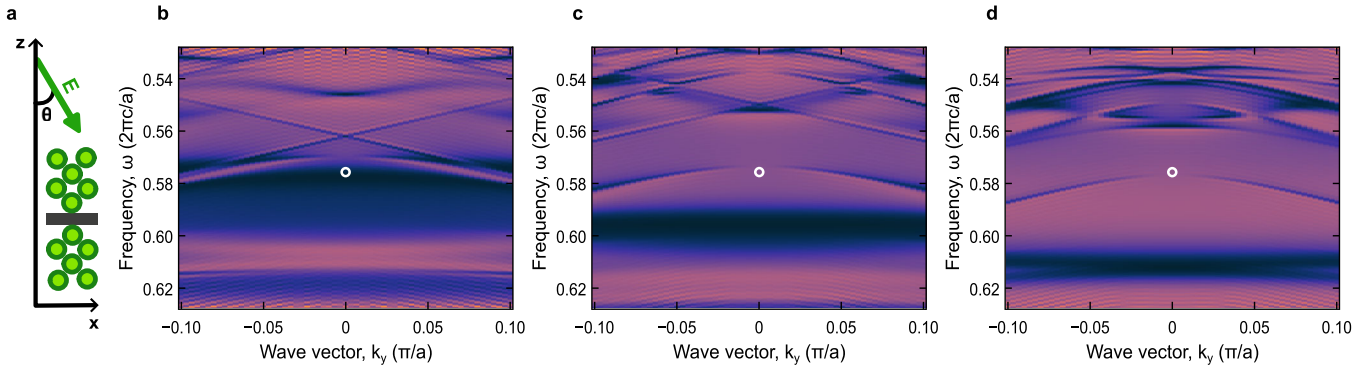


FIGURE 4 | Transmission spectra as a function of tuning across $k_y = 0$, for $k_x = 0.5\pi/a$ (b), $k_x = 0.6\pi/a$ (c), and $k_x = 0.7\pi/a$ (d) for an HCP environment consisting of 6 single-microsphere-thick layers on both sides of the slab. Input light is p-polarized and incident at an angle θ as schematically depicted in (a). All are on the same color scale with arbitrary units. The white circles are the predicted location of the BIC from the FDTD simulations in Figure 2. The insets schematically demonstrate the changing incident angle.

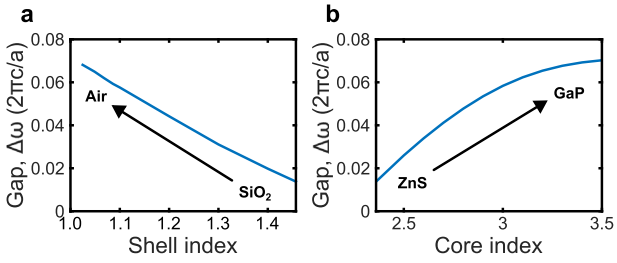


FIGURE 5 | Width of the symmetry bandgap for the FCC microsphere environment at $k_x = 0.8\pi/a$ as the refractive index of the shell material is decreased for fixed ZnS core material (a), and as the index of the core material is increased for fixed SiO_2 shell material.

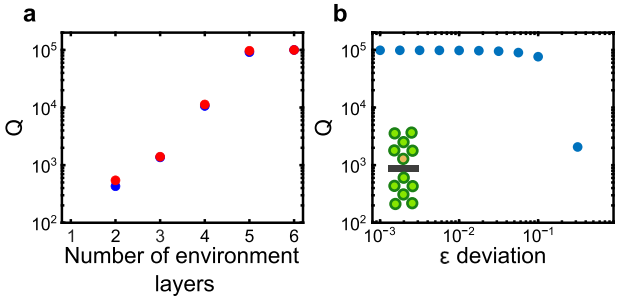


FIGURE 6 | a) Q of the slab-localized BIC at $\mathbf{k}_{\parallel} = (0.75\pi/a, 0)$ as the number of layers of an otherwise pristine HCP environment of microspheres is varied (blue), as well as an HCP environment with one extra R_y-breaking sphere per every four possible spheres placed on top of the topmost layer (red). Any calculated $Q > 10^5$ is shown at 10^5, while no high-Q resonance is found for only a single complete layer of microspheres. b) Q of the mode as a function of ε deviation in the core of a single sphere demonstrating the effects of disorder on the system. The sphere that was adjusted was the one closest to the slab in an FCC lattice (center of the unit cell) on one side of the slab. The inset indicates which sphere had its core ε adjusted.

To quantify the robustness of our approach, we numerically consider a few different forms of structural perturbations. First, we consider the effect of changing the number of layers in an otherwise perfectly crystalline environment to show how many layers are needed to enhance light-matter interactions, shown in Figure 6a. As can be seen, with only three complete layers, the structure only achieves $Q \sim 10^3$, while for four or more complete layers, the Q factor begins to diverge. Moreover, our simulations suggest that any additional microspheres forming an additional incomplete top layer can be effectively ignored relative to an environment containing the same number of complete layers, as the Q of the slab-localized resonance is not substantially altered by their presence, see Figure 6a. Even though any such additional spheres break the system's R_y symmetry, the complete microsphere layers represent a sufficiently thick barrier that exponentially decreases their influence on the slab-localized resonances.

We also consider the effect of disorder in the complete layers of microspheres by introducing controlled perturbations that explicitly break the reflection symmetry of the environment. As shown in Figure 6b, even modest deviations from perfect symmetry only weakly affect the overall response of the system; the nominally infinite Q factors of the line of BICs decrease to large but finite values, which are nevertheless still as large as, or greater than, those typically realized in active metasurfaces [52, 53]. In practice, this means that the relevant slab resonances remain sufficiently isolated from the continuum and light remains strongly confined, despite the unavoidable imperfections in the colloidal crystal. Altogether, these results highlight that the proposed microsphere environment does not require ideal self-assembly to be viable, can be realized with only a few layers of microspheres, and that realistic levels of disorder will still yield high-Q resonances sufficient for active photonic applications.

5 | Conclusion

In this work we have demonstrated a readily fabricated close-packed microsphere structure that supports a line of BICs over a range of frequencies. Indeed, this structure simultaneously supports three such lines of BICs that span the Brillouin zone, due to the rotational and reflection symmetries present in such close-packed sphere structures. As Maxwell's equations are scale invariant, the structure could be scaled up or down to the desired wavelength, within chemical synthesis limits. Moreover, our design represents an attractive approach for coupling

rapid, large-volume assembly methods with conventional active semiconductor materials, which could form the slab subsystem we consider. Specifically, our approach neither requires the microspheres to be active, nor requires any patterning of the semiconductor gain layer, avoiding recombination losses. Although our numerical analysis has focused on TM-like slab-localized resonances, one could instead trap a family of transverse electric-like (TE-like) slab-localized resonances by adjusting the height of the embedded slab. Altogether, we believe this system could have practical applications in tunable high-fidelity filters, rapidly reconfigurable active photonic devices, and a number of other areas.

6 | Methods

6.1 | BIC Location

Modal analysis was performed using MPB [54] on a single unit cell of both FCC and HCP crystal lattices to search for both even and odd modes with respect to the high-symmetry axis. Finite-difference time-domain simulations were performed using MEEP [55] with a rectangular supercell consisting of two unit cells that preserves the reflection symmetry along the **Γ–X** line despite the system's discretization.

6.2 | Transmission Simulations

Transmission spectra were calculated using MEEP [55] using a Guassian source at various incident **k** values. All simulations were run for the same amount of time steps and were normalized against a run with an empty simulation cell.

6.3 | Code Availability

The code that support the findings of this study are available on the archival Purdue Research Repository [56].

Acknowledgements

B.C. acknowledges support from an Energy Frontier Research Center funded by the U.S. Department of Energy (DOE), Office of Science, Basic Energy Sciences (BES), under award DE-SC0025620. A.C. acknowledges support from the Laboratory Directed Research and Development program at Sandia National Laboratories. This work was performed in part at the Center for Integrated Nanotechnologies, an Office of Science User Facility operated for the U.S. Department of Energy (DOE) Office of Science. Sandia National Laboratories is a multimission laboratory managed and operated by National Technology & Engineering Solutions of Sandia, LLC, a wholly owned subsidiary of Honeywell International, Inc., for the U.S. DOE's National Nuclear Security Administration under Contract No. DE-NA-0003525. The views expressed in the article do not necessarily represent the views of the U.S. DOE or the United States Government.

Conflicts of Interest

The authors declare no conflicts of interest.

Data Availability Statement

The data that support the findings of this study are openly available in Purdue Research Repository at https://doi.org/10.4231/9FHB-PW23, reference number 56.

References

1. A. S. Dimitrov and K. Nagayama, "Continuous Convective Assembling of Fine Particles into Two-Dimensional Arrays on Solid Surfaces," *Langmuir* 12, no. 5 (Jan. 1996): 1303–1311.

2. P. Jiang, J. F. Bertone, K. S. Hwang, and V. L. Colvin, "Single-Crystal Colloidal Multilayers of Controlled Thickness," *Chemistry of Materials* 11, no. 8 (Aug. 1999): 2132–2140.

3. Y. Suh, Q. Pham, B. Shao, and Y. Won, "The Control of Colloidal Grain Boundaries through Evaporative Vertical Self-Assembly," *Small* 15, no. 12 (2019): 1804523.

4. P. Jiang and M. J. McFarland, "Large-Scale Fabrication of Wafer-Size Colloidal Crystals, Macroporous Polymers and Nanocomposites by Spin-Coating," *J. Am. Chem. Soc.* 126, no. 42 (Oct. 2004): 13778–13786.

5. A. Mihi, M. Oca na, and H. Míguez, "Oriented Colloidal-Crystal Thin Films by Spin-Coating Microspheres Dispersed in Volatile Media," *Advanced Materials* 18, no. 17 (2006): 2244–2249.

6. M. Banik and R. Mukherjee, "Fabrication of Ordered 2D Colloidal Crystals on Flat and Patterned Substrates by Spin Coating," *ACS Omega* 3, no. 10 (Oct. 2018): 13422–13432.

7. R. C. Hayward, D. A. Saville, and I. A. Aksay, "Electrophoretic Assembly of Colloidal Crystals with Optically Tunable Micropatterns," *Nature* 404, no. 6773 (Mar. 2000): 56–59.

8. A. L. Rogach, N. A. Kotov, D. S. Koktysh, J. W. Ostrander, and G. A. Ragoisha, "Electrophoretic Deposition of Latex-Based 3D Colloidal Photonic Crystals: A Technique for Rapid Production of High-Quality Opals," *Chemistry of Materials* 12, no. 9 (Sept. 2000): 2721–2726.

9. G. T. H. Tran, M. Koike, T. Uchikoshi, and H. Fudouzi, "Fabrication of Polystyrene Colloidal Crystal Film by Electrophoretic Deposition," *Advanced Powder Technology* 31, no. 8 (Aug. 2020): 3085–3092.

10. P. Pieranski, "Two-Dimensional Interfacial Colloidal Crystals," *Physics Review Letters* 45, no. 7 (Aug. 1980): 569–572.

11. M. Bardosova, M. E. Pemble, I. M. Povey, and R. H. Tredgold, "The Langmuir-Blodgett Approach to Making Colloidal Photonic Crystals from Silica Spheres," *Advanced Materials* 22, no. 29 (2010): 3104–3124.

12. A. van Blaaderen, R. Ruel, and P. Wiltzius, "Template-Directed Colloidal Crystallization," *Nature* 385, no. 6614 (Jan. 1997): 321–324.

13. E. Armstrong and C. O'Dwyer, "Artificial Opal Photonic Crystals and Inverse Opal Structures - Fundamentals and Applications from Optics to Energy Storage," *Journal of Materials Chemistry C* 3, no. 24 (June 2015): 6109–6143.

14. Z. Cai, Z. Li, S. Ravaine, et al., "From Colloidal Particles to Photonic Crystals: Advances in Self-Assembly and Their Emerging Applications," *Chemical Society Reviews* 50, no. 10 (May 2021): 5898–5951.

15. K. Busch and S. John, "Photonic Bandgap Formation in Certain Self-Organizing Systems," *Physical Review E* 58, no. 3 (Sept. 1998): 3896–3908.

16. J. E. G. J. Wijnhoven and W. L. Vos, "Preparation of Photonic Crystals Made of Air Spheres in Titania," *Science* 281, no. 5378 (Aug. 1998): 802–804.

17. A. Blanco, E. Chomski, S. Grabtchak, et al., "Large-Scale Synthesis of a Silicon Photonic Crystal with a Complete Three-Dimensional Bandgap near 1.5 Micrometres," *Nature* 405, no. 6785 (May 2000): 437–440.

18. M. He, J. P. Gales, É. Ducrot, et al., "Colloidal Diamond," *Nature* 585, no. 7826 (Sept. 2020): 524–529.

19. S. Fraden and G. Maret, "Multiple Light Scattering from Concentrated, Interacting Suspensions," *Physical Review Letters* 65, no. 4 (1990): 512.

20. R. O. Prum, R. H. Torres, S. Williamson, and J. Dyck, "Coherent Light Scattering by Blue Feather Barbs," *Nature* 396, no. 6706 (Nov. 1998): 28–29.

21. P. Vukusic and J. R. Sambles, "Photonic Structures in Biology," *Nature* 424, no. 6950 (2003): 852–855.

22. S. Kinoshita, S. Yoshioka, and J. Miyazaki, "Physics of Structural Colors," *Reports on Progress in Physics* 71, no. 7 (July 2008): 076401.

23. H. Noh, S. F. Liew, V. Saranathan, et al., "How Noniridescent Colors Are Generated by Quasi-ordered Structures of Bird Feathers," *Advanced Materials* 22, no. 26-27 (Apr. 2010): 2871–2880.

24. L. Shi, Y. Zhang, B. Dong, T. Zhan, X. Liu, and J. Zi, "Amorphous Photonic Crystals with Only Short-Range Order," *Advanced Materials* 25, no. 37 (Oct. 2013): 5314–5320.

25. S. V. Frolov, Z. V. Vardeny, A. A. Zakhidov, and R. H. Baughman, "Laser-Like Emission in Opal Photonic Crystals," *Optics Communications* 162, no. 4 (Apr. 1999): 241–246.

26. M. Shkunov, Z. Vardeny, M. DeLong, R. Polson, A. Zakhidov, and R. Baughman, "Tunable, Gap-State Lasing in Switchable Directions for Opal Photonic Crystals," *Advanced Functional Materials* 12, no. 1 (2002): 21–26.

27. R. V. Nair, A. K. Tiwari, S. Mujumdar, and B. N. Jagatap, "Photonic-Band-Edge-Induced Lasing in Self-Assembled Dye-Activated Photonic Crystals," *Physical Review A* 85, no. 2 (Feb. 2012): 023844.

28. Y. A. Vlasov, N. Yao, and D. J. Norris, "Synthesis of Photonic Crystals for Optical Wavelengths from Semiconductor Quantum Dots," *Advanced Materials* 11, no. 2 (1999): 165–169.

29. P. Lodahl, A. Floris van Driel, I. S. Nikolaev, et al., "Controlling the Dynamics of Spontaneous Emission from Quantum Dots by Photonic Crystals," *Nature* 430, no. 7000 (Aug. 2004): 654–657.

30. A. S. Schulz, M. Kozoň, G. J. Vancso, J. Huskens, and W. L. Vos, "Strongly Inhibited Spontaneous Emission of PbS Quantum Dots Covalently Bound to 3D Silicon Photonic Band Gap Crystals," *Journal of Physical Chemistry C* 128, no. 22 (June 2024): 9142–9153.

31. J. Gomis-Bresco, D. Artigas, and L. Torner, "Anisotropy-Induced Photonic Bound States in the Continuum," *Nature Photonics* 11 (Mar. 2017): 232.

32. S. Mukherjee, J. Gomis-Bresco, P. Pujol-Closa, D. Artigas, and L. Torner, "Topological Properties of Bound States in the Continuum in Geometries with Broken Anisotropy Symmetry," *Physical Review A* 98, no. 6 (Dec. 2018): 063826.

33. A. Cerjan, C. W. Hsu, and M. C. Rechtsman, "Bound States in the Continuum through Environmental Design," *Physical Review Letters* 123, no. 2 (July 2019): 023902.

34. A. Cerjan, C. Jörg, S. Vaidya, et al., "Observation of Bound States in the Continuum Embedded in Symmetry Bandgaps," *Science Advances* 7 (Dec. 2021): eabk1117.

35. L. Yang, R. Zheng, S. Zhang, et al., "Lines of Bound States in the Continuum in a Phononic Crystal Slab," *Physical Review B* 111, no. 13 (Apr. 2025): 134102.

36. C. W. Hsu, B. Zhen, A. D. Stone, J. D. Joannopoulos, and M. Soljačić, "Bound States in the Continuum," *Nature Reviews Materials* 1 (July 2016): 16048.

37. P. Paddon and J. F. Young, "Two-dimensional vector-coupled-mode theory for textured planar waveguides," *Physical Review B* 61 (Jan. 2000): 2090–2101.

38. V. Pacradouni, W. J. Mandeville, A. R. Cowan, P. Paddon, J. F. Young, and S. R. Johnson, "Photonic band structure of dielectric membranes periodically textured in two dimensions," *Physical Review B* 62 (Aug. 2000): 4204–4207.

39. T. Ochiai and K. Sakoda, "Dispersion relation and optical transmittance of a hexagonal photonic crystal slab," *Physical Review B* 63 (Mar. 2001): 125107.

40. S. Fan and J. D. Joannopoulos, "Analysis of guided resonances in photonic crystal slabs," *Physical Review B* 65 (June 2002): 235112.

41. Y. Plotnik, O. Peleg, F. Dreisow, et al., "Experimental Observation of Optical Bound States in the Continuum," *Physical Review Letters* 107 (Oct. 2011): 183901.

42. J. Lee, B. Zhen, S.-L. Chua, et al., "Observation and Differentiation of Unique High-Q Optical Resonances Near Zero Wave Vector in Macroscopic Photonic Crystal Slabs," *Physical Review Letters* 109, no. 6 (Aug. 2012): 067401.

43. H. Friedrich and D. Wintgen, "Interfering Resonances and Bound States in the Continuum," *Physical Review A* 32 (Dec. 1985): 3231–3242.

44. S. I. Azzam, V. M. Shalaev, A. Boltasseva, and A. V. Kildishev, "Formation of Bound States in the Continuum in Hybrid Plasmonic-Photonic Systems," *Physical Review Letters* 121 (Dec. 2018): 253901.

45. C. W. Hsu, B. Zhen, S.-L. Chua, S. G. Johnson, J. D. Joannopoulos, and M. Soljačić, "Bloch Surface Eigenstates within the Radiation Continuum," *Light: Science & Applications* 2 (July 2013): e84.

46. C. W. Hsu, B. Zhen, J. Lee, et al., "Observation of Trapped Light Within the Radiation Continuum," *Nature* 499 (July 2013): 188–191.

47. K. Sakoda, *Optical Properties of Photonic Crystals* (Berlin, New York: Springer, 2005).

48. A. C. Overvig, S. C. Malek, M. J. Carter, S. Shrestha, and N. Yu, "Selection Rules for Quasibound States in the Continuum," *Physical Review B* 102, no. 3 (2020): 035434.

49. N. X. V. Lan, J. Moon, T. H. Kang, K. Wang, H.-G. Park, and G.-R. Yi, "Index-Matched Composite Colloidal Crystals of Core-Shell Particles for Strong Structural Colors and Optical Transparency," *Chemistry of Materials* 33 (Jan. 2021): 1714–1722.

50. T. A. Welling, K. Kurioka, H. Namigata, K. Suga, D. Nagao, and K. Watanabe, "Highly Reflective and Transparent Shell-Index-Matched Colloidal Crystals of Core–Shell Particles for Stacked RGB Films," *ACS Applied Nano Materials* 7, no. 16 (2024): 18337–18345.

51. Y. Fu, H. Zhao, Y. Wang, D. Chen, Z. Yu, J. Zheng, S. Sun, W. Cai, and H. Zhou, "Reversible Photochromic Photonic Crystal Device with Dual Structural Colors," *ACS Applied Materials & Interfaces* 14, no. 25 (2022): 29070–29076.

52. C. U. Hail, M. Foley, R. Sokhoyan, L. Michaeli, and H. A. Atwater, "High Quality Factor Metasurfaces for Two-Dimensional Wavefront Manipulation," *Nature Communications* 14, no. 1 (Dec. 2023): 8476.

53. N. Muhammad, Z. Su, Q. Jiang, Y. Wang, and L. Huang, "Radiationless Optical Modes in Metasurfaces: Recent Progress and Applications," *Light: Science & Applications* 13, no. 1 (Aug. 2024): 192.

54. S. G. Johnson and J. D. Joannopoulos, "Block-Iterative Frequency-Domain Methods for Maxwell's Equations in a Planewave Basis," *Optics Express* 8, no. 3 (Jan. 2001): 173–190.

55. A. F. Oskooi, D. Roundy, M. Ibanescu, P. Bermel, J. D. Joannopoulos, and S. G. Johnson, "Meep: A Flexible Free-Software Package for Electromagnetic Simulations by the FDTD Method," *Computer Physics Communications* 181, no. 3 (Mar. 2010): 687–702.

56. B. Cerjan and A. Cerjan, "Lines of Bound States in the Continuum in Monodisperse Microsphere Structures [Repository]," 2025, https://doi.org/10.4231/9FHB-PW23.